Observations of high-energy radiation during thunderstorms at Tien-Shan

A. V. Gurevich,[1,*] A. M. Almenova,[2] V. P. Antonova,[3] A. P. Chubenko,[1] A. N. Karashtin,[4] O. N. Kryakunova,[3] V. Yu. Lutsenko,[3] G. G. Mitko,[1] M. O. Ptitsyn,[1] V. V. Piscal,[1,5] V. A. Ryabov,[1] N. M. Salikhov,[3] T. Kh. Sadykov,[2] A. L. Shepetov,[1] Yu. V. Shlyugaev,[6] W. M. Thu,[7] L. I. Vil'danova,[1,5] N. N. Zastrozhnova,[2] and K. P. Zybin[1]

[1]*P.N. Lebedev Physical Institute of the Russian Academy of Sciences (FIAN), 119991 Leninskii pr., 53, Moscow, Russia*

[2]*Institute for Physics and Technology, Almaty, 050032 Ibragimova, 11, Kazakhstan*

[3]*Institute of Ionosphere, 050020 Kamenskoye plato, Almaty, Kazakhstan*

[4]*Radiophysics Research Institute, Nizhny Novgorod State University, 603950 Bol'shaya Pechyorskaya, str., 25/12a, Nizhny Novgorod, Russia*

[5]*Tien Shan Mountain Cosmic Ray Station, 050020 Mitina str., 3, Almaty, Kazakhstan*

[6]*Institute of Applied Physics of RAS, 603950 Ul'yanova str., 46, Nizhny Novgorod, Russia*

[7]*Moscow Institute of Physics and Technology (State University), 117303 Moscow, Russia*

(Received 3 March 2016; published 6 July 2016)

Energetic radiation during thunderstorms is studied. The possibility to identify the high-energy lightning emission in the 10 s monitoring mode is demonstrated. Simultaneous measurements of gamma-ray emission, high-energy electrons, and neutron radiation in the triggering mode are fulfilled. Energy spectra of gamma emission and electrons are obtained. The intensity both of electrons and gamma rays in lightning discharge prevail the background emission by 1.5 to 2 orders of magnitude.

DOI: 10.1103/PhysRevD.94.023003

I. INTRODUCTION

The intensive gamma emission during a thunderstorm was first observed inside thunderclouds [1,2]. Afterward, multiple on-ground observations were fulfilled [3,4] (see Refs. [5,6]). The high-energy electron spectrum measurements [7] and detailed studies using the lightning triggering method [8] could be specially mentioned.

The high-energy radiation observed during a thunderstorm is of two types. One is a long-period emission lasting some tens of minutes or even hours. Another is a short one but very intensive. It lasts less than a second, and usually the main part of this emission lasts even a few milliseconds.

The emission of the first type is connected with thunderclouds. It is usually supposed to be determined mainly by the emanation of radioactive gases (Rn or Rn daughter). This long-period emission gives the main input into the high-energy emission of the thunderstorm. It is observed in monitoring mode measurements using 5 min time intervals usually. The short-time emission was observed previously only in a triggering mode using lightning as a trigger.

In the paper, we demonstrate that the lightning high-energy emission could be directly observed in the monitoring mode. To achieve this, the monitoring time interval was diminished down to 10 s. The results are confirmed by the simultaneous triggering mode measurements.

The wide complex of measurements in a triggering mode was fulfilled. The spectrum of lightning gamma emission was obtained. Together with gamma, the relativistic high-energy electrons are observed. The energy spectrum of electrons is registered up to tens of MeV. The gamma and electron high-energy spectra are obtained simultaneously in multiple lightning events.

Additionally, the lightning neutron emission was registered. It was shown to consist both of low-energy neutrons and of the intensive flow of energetic neutrons.

II. INSTRUMENTATION

The experimental complex Groza (i.e., "Thunderstorm") is designed for investigation of the high-energy radiations which accompany the lightning development in thunderclouds. It is situated at the scientific cosmic-ray station in the mountains of Northern Tien-Shan, 3340 m above sea level, just at an altitude which corresponds to the local altitude of thunderclouds movement [9–11]. During its rather prolonged history and constant development, the configuration of the detector system was steadily modified, and at the present time, it consists of the following.

The registration of the low-energy gamma- and X-ray radiation succeeds due to a set of scintillation detectors based on the inorganic NaI scintillator crystal which is coupled with a FEU49-type photomultiplier tube (PMT). Internal arrangement of such a detector is shown in Fig. 1. The scintillation crystal is of cylindrical shape with the sizes Ø110 × 110 mm; together with PMT, it is put inside an electrically grounded aluminum casing with the 1 mm wall thickness.

Electric signals from the PMT anode with its amplitude being proportional to the energy of registered gamma-quantum are transmitted in parallel to the set of pulse

*alex@lpi.ru

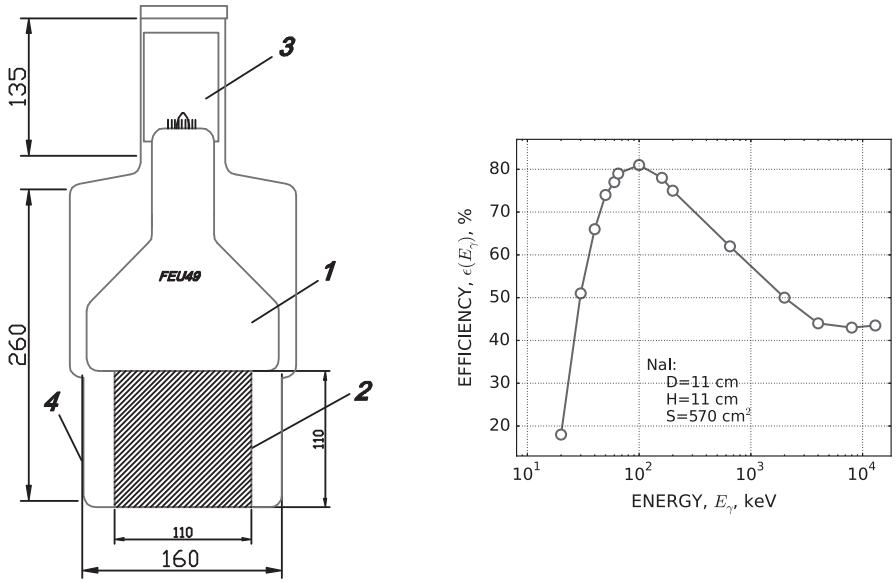

FIG. 1. Left: internal arrangement of the scintillation gamma detector: *1*—PMT, *2*—NaI crystal, *3*—electronics board, *4*—external 1 mm thick aluminum housing. Right: the gamma-ray registration efficiency with the NaI crystal used in the Groza experiment (Geant4 simulation). Dimensions are shown in millimeters.

discriminators with consecutively increasing operation thresholds. At time, up to 8–12 amplitude discriminators are used with every scintillation detector, their thresholds being equivalent to gamma-radiation energies varying in the range of 30–2000 keV. The standard digital pulses from discriminator outputs are connected to the multichannel computer-driven scaler board, which permits tracing the time history of gamma-radiation intensity synchronously in different energy ranges. The series of pulse counts is measured by an electronic scaler board simultaneously in two diapasons of time resolution, low- (1–10 s) and a high-resolution (50–200 μs) ones; in the latter case, the sum duration of the uninterruptable high-resolution signal record T_r can be stretched up to 1–5 s. The scaler system keeps constantly in its internal memory the time history of input pulse intensity measured during the lapse of the last T_r interval, and can write it down with the arrival of a special control signal—the trigger. In intensity records obtained with this system, the arrival moment of the trigger signal coincides always with the median of the written time history, i.e., with the $T_r/2$ moment. So, the first half of every record corresponds to the prehistory of intensity development in the period before the trigger arrival, and the second half corresponds to the after trigger time.

The low-resolution intensity measurements are kept continuously without any binding to some control signal; these data are used for a steady check of the detector operation consistency and for monitoring of the background environmental radiations around the point of detector placement.

Absolute energy calibration of the NaI scintillators is performed with the use of a ^{241}Am and ^{137}Cs gamma-ray sources. The detector's energy resolution defined as a half-width of a full absorption peak is estimated to be about 60% around the cesium peak (660 keV) and about 40%–50% in the range of americium energies (20–30 keV). Also, operation of a NaI crystal scintillator in real geometry of the Groza experiment is checked with the simulation made on the basis of the Geant4 package [12]. The right plot of Fig. 1 presents simulation results for energy dependence of the gamma-ray registration efficiency with typical NaI scintillator used in our experiment. It is seen that for the keV energy range radiation the scintillator ensures a rather high efficiency of the order of some tens of percent, which permits compensating its low aperture caused by a comparatively small sensitive area of the crystal.

For registration of the high-energy (above some MeV) gamma rays together with charged particles accelerated by an electric field in thunderclouds, the special large-size ionization detectors are used at Tien-Shan station. The detectors are built on the basis of SI5G-type Geiger-Müller tubes operating with reduced high-voltage feeding in the proportional mode. As calibration measurements with a set of radioactive sources have shown, these counters are mostly sensitive to the charged relativistic particles which are registered with a 95%–99% efficiency, while their efficiency relative to gamma radiation of MeV range energies varies in the limits of 0.05%–1% (see the right plot in Fig. 2). Hence, the ionization detectors are complimentary to the crystal scintillators, and permit to select the signal from charged particles against a much more intensive background of the scattered electromagnetic radiation.

The cross-cut of the ionization detector is shown on the left drawing of Fig. 2. The SI5G-type counters are grouped

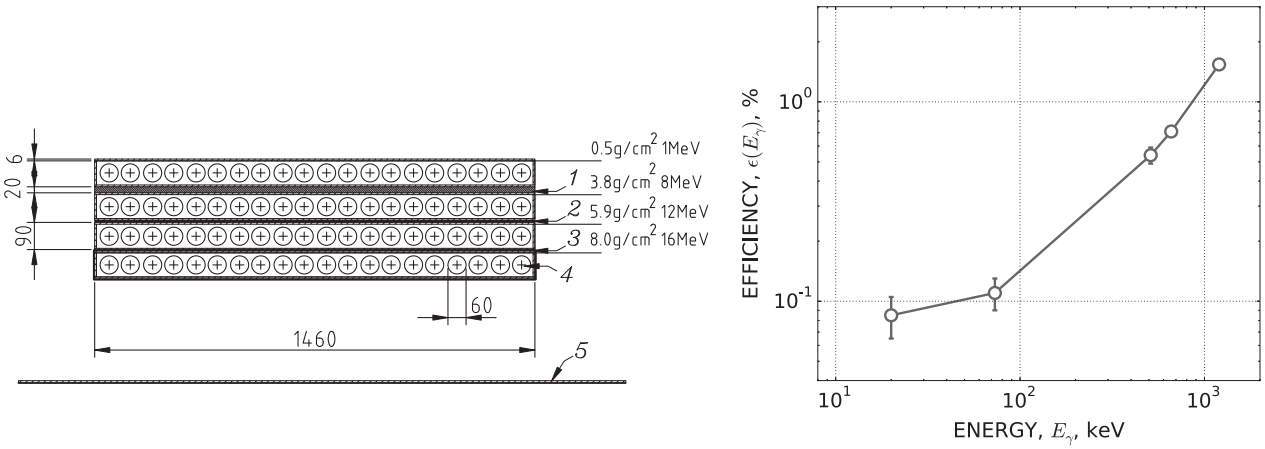

FIG. 2. Left: internal arrangement of ionization spectrometer: *1*—rubber, *2* and *3*—lead sheets, *4*—the Geiger-Müller counter, *5*—the lower 5 mm thick lead shielding. Right: the gamma-ray registration efficiency for a single ionization counter (calibration measurements). Dimensions are shown in millimeters.

by 20 pieces into a box with the walls made of 1 mm thick aluminum and with 5 mm thick plywood tops; the walls of counter tubes are glass and have 1 mm thickness. Output pulses of all 20 counters in a box are connected in parallel to the common signal cable so every box corresponds to a single informational channel. The length of the cathode coating inside the SI5G-type tube is about 560 mm with a 60 mm diameter, and hence the 20-tube box provides an effective sensitive area of about 0.67 m^2 (for a vertically directed particle flow).

As seen in Fig. 2, the counter boxes of the ionization detector are stacked pilewise, four counter layers in every vertical pile, and a number of lead and rubber absorber sheets are placed between the boxes in a pile. Such a setup converts the detector into a full absorption spectrometer, which permits estimating roughly the energy of the registered particle due to the presence or absence of its signal in subsequent counter layers. The structure of absorber layers, their sum thickness, and corresponding energy thresholds (for vertically going relativistic particles) are shown in Fig. 2; a ~ 2 g/cm^2 roof thickness of a wooden cabin where detector setups are hosted should be added to the matter depth above every layer. An additional 3 mm thick sheet of lead spread beneath the lower counter box shields the detector from upward-going scattered gamma radiation.

At the time of the discussed experiment, two ionization detector points, ID1 and ID2, were operating at Tien-Shan mountain station; both of them had three piles of four vertically arranged counter boxes inside a light plywood cabin. Hence, the sum sensitive area of every counter layer in a point was about 2 m^2. Detector points ID1 and ID2 were situated on the level of Tien-Shan station at the distance of about 160 m from each other. The line connecting these points was roughly perpendicular to usual direction of thundercloud movement.

Output pulses of all ionization tubes constituting every counter layer inside a detector point are connected to one and the same cable line, which is used for their transmission to the data registration center. Hence, four pulse signals come into this center from each detector point; these are the signals from its upper, two intermediate, and lower counter layers. Another three information signals are the pulses of successive coincidences $1+2$, $1+2+3$, and $1+2+3+4$ between subsequent counter layers of the detector point. Because of the strong difference in the registration probability of charged and neutral particles, the coincidence signals correspond mostly to the passages of charged particles through detector pile and permit selecting effectively the electron component among all radiation flows generated in a thundercloud.

All information signals from ionization detector come to the same multichannel scaler board and are registered just in the same way as applied for the acquisition of scintillation data, i.e., with registration of both the low-resolution intensity monitoring records without any definite time binding and the high-resolution time series of signal pulses relative to an external control signal—the trigger.

Besides the radiation of electromagnetic type from thunderclouds, the search for a lightning-correlated neutron signal was done during the last measurement seasons at Tien-Shan. A number of neutron detectors effective in different ranges of neutron energy, from thermal energy and up to the values of the order of some MeV are used for this purpose (see Fig. 3); this detector system together with the results on neutron registration are described in detail in our works [13] and [14]. The intensity of the neutron signal is registered in the same way as by other detector types: the low-resolution monitoring data are written together with the high-resolution records bound to an external lightning trigger.

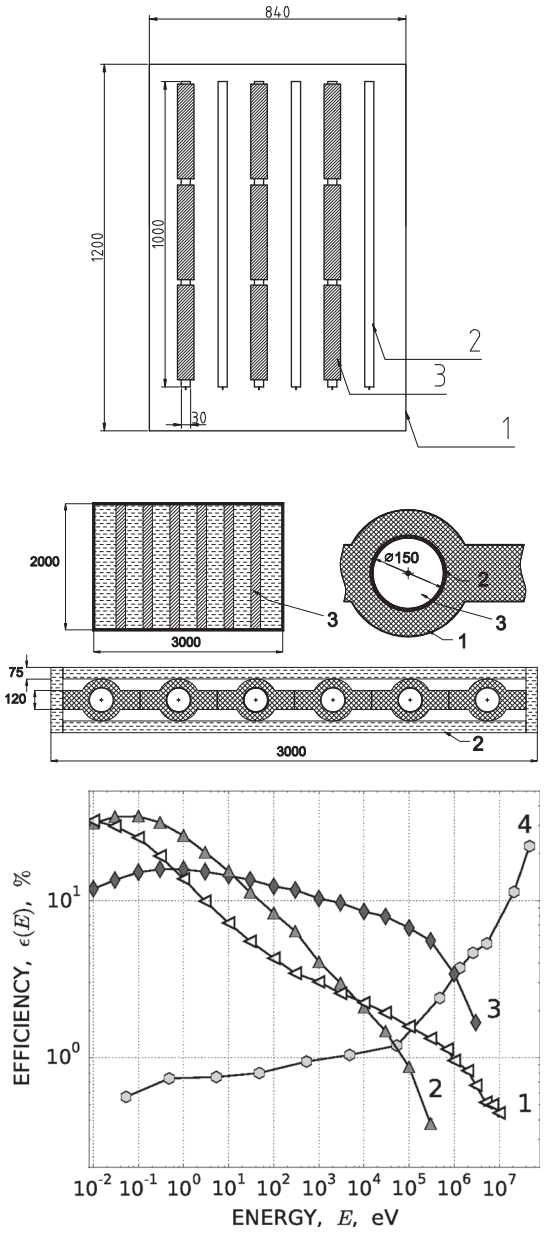

FIG. 3. Neutron detection in the Groza experiment. Top: the low- and intermediate-energy detector (*1*—1 mm thick wall of an aluminum box, *2*—the proportional neutron counter "Helium-2," and *3*—polyethylene moderator tubes). Middle: the NM64-type neutron monitor used for registration of the high-energy neutrons (*1*—lead, *2*—polyethylene, and *3*—the SNM15-type proportional neutron counter). Bottom: the energy dependence of the neutron registration efficiency (Geant4 simulation; *1*—for a six "Helium-2" counters box without any moderator, *2* and *3*—for the counters inside a moderator tube with wall thickness of 0.5 cm and 1 cm; *4*—for the NM64 neutron monitor).

Both neutrons and MeV range gamma radiation could be registered with proportional counters. As a mean against misinterpretation of counter signals caused by gamma radiation as caused by neutrons all boxes of low-energy neutron detector have outer screening made of 1 mm thick lead sheets. As for the NM64-type supermonitor which is used for the detection of the high-energy neutron component, its counters are just within internal lead tubes with the wall thickness about 10 cm, which plays the role of gamma-radiation absorber. Besides, as the special Geant4 simulation of the complex physical processes which take place in detectors of the considered type has shown, their efficiency relative to electromagnetic components achieves some noticeable value about 1% only above the gamma-ray energy of 10–30 MeV; below this energy range, the probability of neutron registration prevails by many orders of magnitude. A more detailed description of neutron detectors of the Tien-Shan station and the discussion of their background can be found in Ref. [14].

A set of radio antennas operating in the 0.3–1 MHz frequency range together with a corresponding receiver and fast ADC system is used for registration of close lightning discharges through their radio emission over the time gap ± 0.15 s around the lightning [15]. Simultaneously, the amplified signal from the radio receiver comes to a threshold discriminator scheme which generates the trigger pulse just in the beginning moment of discharge. This trigger is transmitted to all registration subsystems of the *Groza* installation and is used there for the synchronization of the high-resolution records of detector signals.

The strength of the near-Earth electric field in thunderstorm periods is measured by the "field-mill" type field sensor. The quasi-potential output voltage of this sensor is digitized and recorded also in two modes, the low-resolution continuous monitoring, and high-resolution triggered ones, similarly to registration of the pulse intensities from radiation detectors. Another electric filed detector of a capacitor type with a grounded plate is used for registering the moments of the fast field variations around the times of nearby discharges. Also, the standard weather station provides continuous measurements of pressure, temperature, the amount of precipitation, and other atmospheric parameters.

The direction and linear distance from the detector site to the region of atmospheric discharge in thunderstorms is roughly estimated through the time delay of accompanying sound, which is measured by a distributed set of microphones synchronized with a general lightning trigger signal.

The present disposition of the Groza detector complex on the territory of the Tien-Shan station is shown in Fig. 4.

For comparison of the results on the intensity of particle detector signals obtained experimentally with what should be expected for particle flows originated in thunderclouds according to existing models of particle interaction, the development process of an electron-photon avalanche inside a large-scale electric field was simulated with the use of the Geant4 simulation toolkit. For this purpose, a simple simulation model which takes into account the characteristic features of the Tien-Shan experiment was

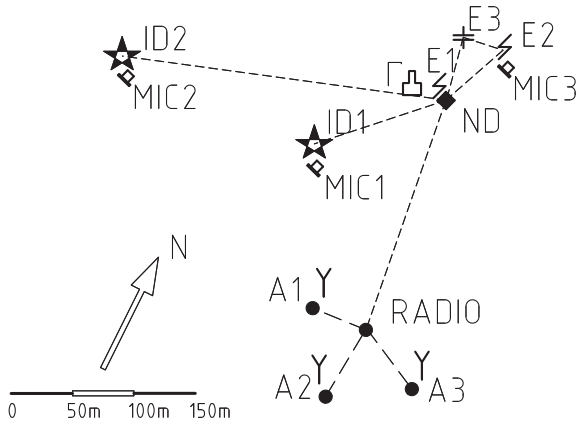

FIG. 4. Schema of the detector complex used in the present experiment. *ID1* and *ID2*—ionization detectors; Γ—scintillation detector of the low-energy gamma rays; *ND*—the neutron detector complex; *A1–A3*—radio antennas; *E1–E3*—electric field sensors; *MIC1–MIC3*—acoustic sensors of the thunder sound.

built: a $5 \times 5 \times 5$ km^3 volume $\mathcal{V}$ was supposed to be filled by the air with standard gas content (75.5 mass percent of N, 23.2% O, 1.28% Ar, and 0.01% C) and exponentially decreasing height dependence of its pressure and density; the air pressure on the "bottom" side of this volume was taken to be 675 mb, which corresponds to the average atmospheric pressure at the level of the Tien-Shan station. The presence of an electric field in a thundercloud was imitated with a cylindrical spatial region, 3 km in the height and 1.5 km in diameter, where the homogeneous electric field was set with the corresponding tools of the Geant4 package. The direction of this field ensured acceleration of negatively charged particles (electrons) toward the bottom surface, and the center of the cylindrical thundercloud field region coincided with the geometrical center of the considered volume $\mathcal{V}$. In each simulation run the seed electrons were placed just in this center point, the directions of their initial speeds were uniformly distributed. The development of the avalanche was followed through tracing the trajectories of all electrons.

The set of physical models included in simulation involved the common processes of electromagnetic physics: the bremsstrahlung, multiple scattering, and ionization losses for electrons; the photo and Compton effects and the pair production for gamma radiation; and the positron annihilation. Since the presence of low-energy charged particles which could be accelerated by the field is crucial for the task, we were interested in the trajectories of both electrons, and gamma-quanta were traced until their kinetic energy fell down to a rather low threshold of 100 eV (due to ionization losses and the photo effect correspondingly). At the same time, only the particles with energy above 30 keV at the final point of their trajectory were included in the output set of the simulated avalanche products. The energy corresponds to the *Groza* complex lower registration limit of some tens keV.

III. RESULTS

A. Low-resolution measurements in monitoring mode

During the longstanding realization of the Groza experiment, a multitude of storm events was observed at the Tien-Shan mountain station, and most of them constantly demonstrated one and the same characteristic features in the monitoring data of radiation activity. A typical example of such events is presented in Fig. 5 where intensity records for the signals from a number of radiation detectors (the gamma-radiation crystal scintillator, four ionization detector layers, and the mutual coincidences between the latter) are shown together with the data on the near-Earth electric field and the minute amount of precipitation fallout. The distributions of radiation intensity in Fig. 5 are normalized to the number of detector pulse signals N_p which was accepted during the standard 10 s long exposition time.

Two kinds of characteristic signal irregularities which are generally typical for every thunderstorm period could be seen in the monitoring records of the Fig. 5. First, there are the comparatively prolonged increases in radiation intensity, all having a relaxation time of the order of some tens of minutes. As seen in the left frame of Fig. 5, these slow enhancements are mostly prominent in the signal of the NaI crystal scintillator, which is sensitive generally to the low-energy gamma rays. Also, an obvious correlation between the beginnings of precipitation fallout and the start moments of long-term gamma-radiation growth is steadily seen in the figure.

Because of all mentioned features—its gamma-ray nature, a connection with the precipitation moments, and the nearly constant relaxation time after a relatively sharp initial extremum—the long term surplus radiation can be supposed to be originating from additional temporary entry of some radioactive gases, probably radon and its disintegration products into the near-Earth atmosphere, which usually attend the precipitations [16–18]. Especially for the environment of the Tien-Shan station, this effect is investigated more precisely in our work [19].

Another temporary feature abundantly seen at stormy times in monitoring records are the short spikelike bursts of radiation intensity (see Fig. 5). Namely, it was distinctly seen that the bursts could be easily traced in the signal of the gamma detector, in separate counter layers of the ionization detector, and in the coincidence signal between the layers. It means that both gamma spikes and energetic electron spikes were registered. The characteristic duration of the spikes clearly seen in the expanded Fig. 6 is 10 s—exactly equal to one exposition interval of the monitoring process. One can see from the figure that the short time bursts are closely connected with the lightning triggers. It means that in a 10 s monitoring mode we directly observed the high-energy gamma emission of lightning.

Lightning is a very short and very intensive phenomenon. Its gamma emission lasts a few milliseconds only. But

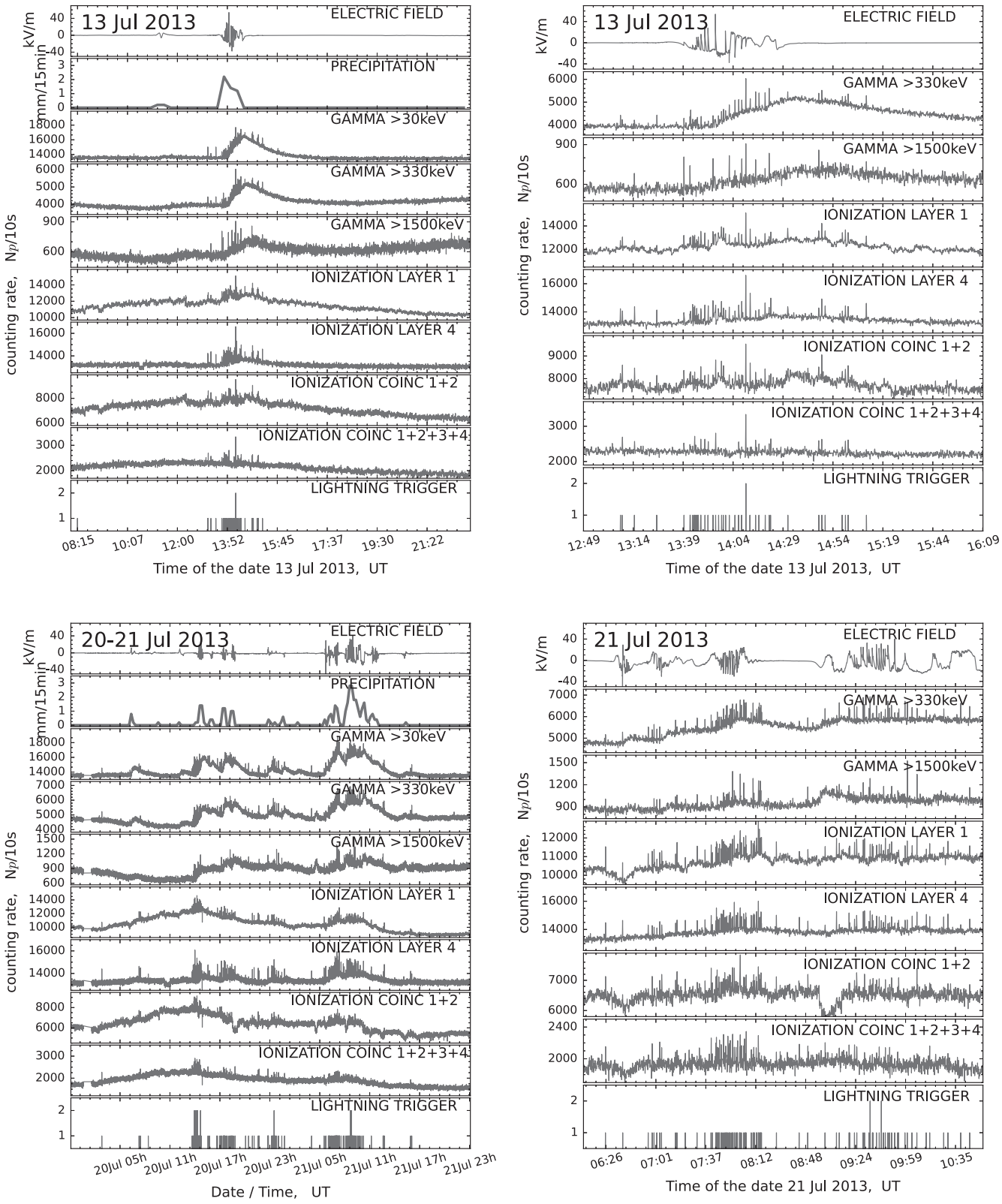

FIG. 5. Two typical stormy periods happened on 13 and 20–21 July 2013. Left frames: 10s-resolution monitoring records of electric field, precipitation, the gamma-ray intensity, and the intensity of ionization detector signals. Right frame: same distributions stretched around the time of intensive nearby storm when multiple transient short-time bursts were seen among radiation signal.

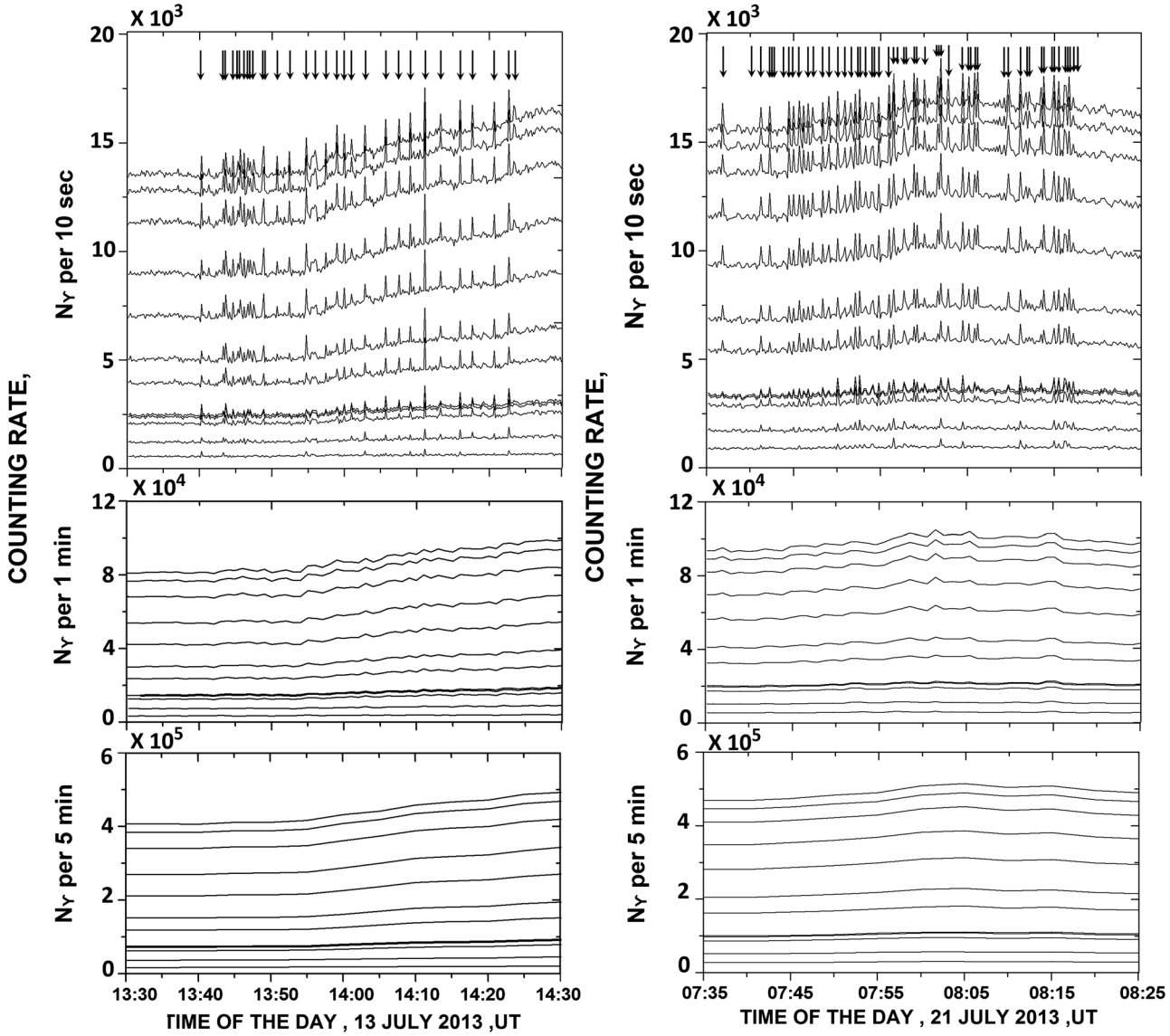

FIG. 6. Examples of gamma-ray flashes seen in 10 s monitoring mode. In every column from top down: 10 s, 1 min and 5 min monitoring mode. Twelve curves in each panel present gamma-ray count rates for different gamma-ray energy thresholds. From top to down: > 30 keV, > 50 keV, > 80 keV, > 110 keV, > 160 keV, > 240 keV, > 330, > 420 keV, > 510 keV, > 600 keV, > 960 keV, > 1500 keV. Arrows at the top of the figure indicate the trigger moments.

its intensity is orders of magnitude higher than the background. That is why lightning gamma bursts were clearly seen in the 10 s monitoring. Note that in the longer monitoring mode the lightning gamma emission became nonpronounced and practically could not be detected. It is seen from Fig. 6.

Note that the intensity of gamma bursts seen in the 10 s monitoring mode generally decreases with energy, Fig. 6. But, in a part of the bursts (20%) the relation of the amplitude to the gamma background increases with energy and reaches a value of about 50% at the highest observed energy 1.5 MeV.

Thus, we see that lightning could be diagnosed by its high-energy emission in 10 s monitoring. For a detailed study, a high-resolution triggering method should be used.

B. High-resolution time measurements

The next step ahead from the monitorlike intensity recording would be the registration of detector signal intensities with resolution enhanced up to the milli- and microsecond time range and with a strict binding of these detailed measurement series to a precise moment of atmospheric discharge. This issue is addressed now at the Tien-Shan station by its system of multichannel pulse intensity measurements operating with the 100–200 μs time resolution and synchronized immediately by a trigger signal from the radio antenna of discharge registration.

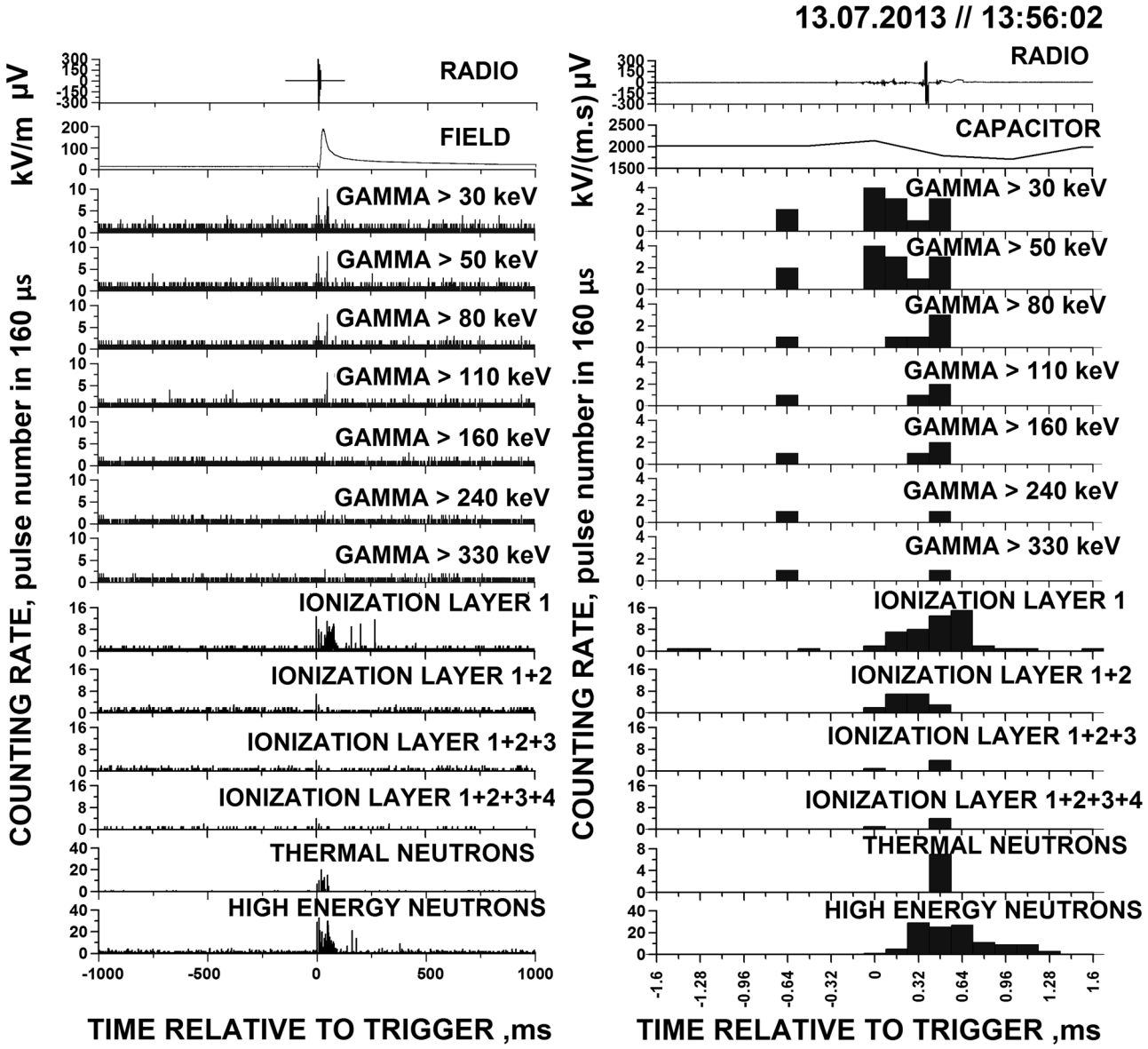

FIG. 7. The high-resolution time history of signal intensities registered in a close lightning event on July 13, 2013. Left frames, from top to bottom: the root-mean-square amplitude of the discharge radio emission on antenna input, the strength of the near-Earth electric field, and the pulse counting rate in different types of particle detectors (see the text). Right frames: same distributions stretched around the moment of the lightning trigger (slow record of the averaged field is changed by the fast field variation signal from the capacitor sensor).

Two typical samples of the events registered by close lightning discharges are shown in Figs. 7 and 8. The data presented here were measured with the 0.02 μs (for the radio signal), 188 μs (for the electric field), and 160 μs (for all detector pulse counting rates) time granularity.

The time history of atmospheric discharge in both events of Figs. 7 and 8 can be traced precisely through the fast record of the radio signal emitted immediately by the lightning; generally, the beginning of every lightning discharge is accompanied with a simultaneous sharp change of the local electric field. The linear distance from the discharge region in thunderclouds to our detector set can be appreciated by microphone records of a thunder report from Fig. 9; taking the usual estimation of sound velocity about 0.3 km/s, these records correspond to distances within the range of 0.6–1 km from the lightning channel.

In the case of thundercloud passage close enough to the detector set, the fast transient outbursts (both the gamma and electron ones) were frequently seen during the lightning initiation—the initial breakdown marked by the first strong bursts of HF radio emission. A number of such outbursts can be found on the two left frames of Figs. 7 and 8. It is seen that these outbursts coincided with

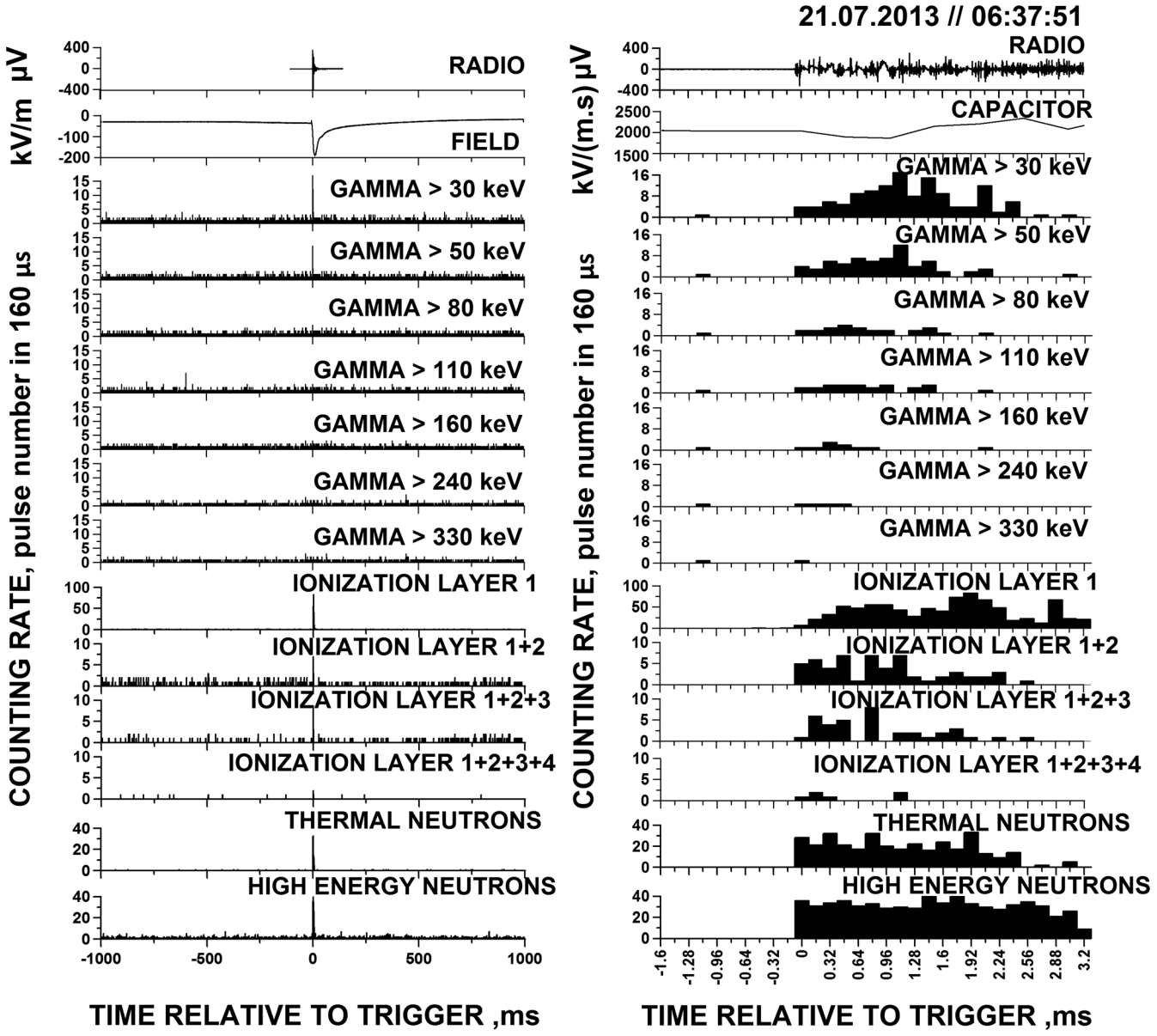

FIG. 8. Same distributions as in Fig. 7 for another discharge event that happened on July 21, 2015.

lightning initiation and usually had a very sharp abrupt shape, typically of 1–5 time extents of the measurement period, i.e., of 150–800 μs. Radiation bursts of this type were present both in the signal from the low-energy crystal scintillator, from ionization counter detectors, and in coincidence signals between succeeding ionization layers. Additionally, short and rare gamma bursts were seen sometimes during the whole discharge time; they were possibly related to lightning leader emission.

The ionization detector had four counter layers. Because of a low probability for every particular gamma quantum to be registered by a single counter layer, the presence of noticeable coincidence signal from the short-time radiation burst was a plain sign of the presence of energetic charged particles (evidently, electrons accelerated inside the electric field of a thundercloud) among the short-time enhancement of the particle flux; the possibility to see clearly the transient increase in the signal of four-times coincidence between successive layers means that the energy of these accelerated particles must have been at least about some tens of MeV.

The two lower plots in all frames of Figs. 7 and 8 present the time distributions of neutron intensity measured with two separate types of neutron detectors in the range of thermal energy (~0.025 eV) and in the high-energy range $\geq$1 MeV (see Ref. [14] for details). A prominent increase of neutron flux was seen in both energy ranges just around the time of the atmospheric electric discharge.

The possibility of neutron production inside the developing electron-photon avalanche in the atmosphere was

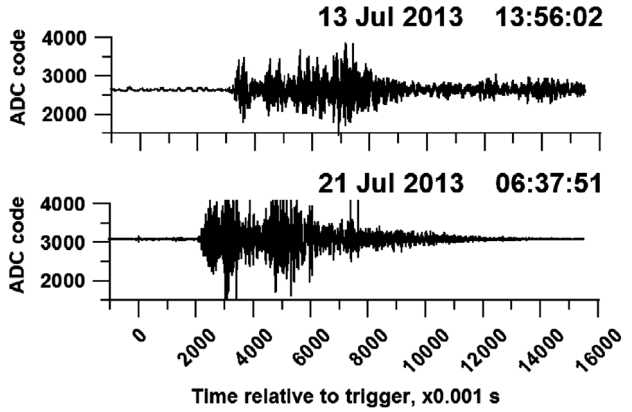

FIG. 9. Microphone records of thunder sound taken in two events from Figs. 7 and 8.

ensured by the means of photo- and electronuclear reaction models from the standard Geant4 distribution. The simulation took into account elastic and inelestic neutron collisions for low (0.01–4 eV), intermediate (4 eV–20 MeV), and high (above 20 MeV) energies, and radiative neutron capture.

The observation results demonstrate that the neutron flux was 2 orders of magnitude higher than predicted by the model. So, the considered physical processes do not explain the observed neutron flux.

C. Energy spectra of registered radiation

The whole set of signal intensity distributions from Figs. 7 and 8, which have been obtained with a number of energy thresholds can be used for estimation of the energy spectrum of additional transient particle flux responsible for the sharp radiation bursts accompanying the close lightning discharges on the micro- and millisecond time scale. In the two right frames of this figure, intensity distributions are stretched around the zero point of the time axis, which coincides with the lightning trigger moment, so the number of additional pulses can be immediately counted over the space of transient burst both for the NaI gamma scintillator and all channels of the ionization detector. Taking into account the corresponding energy thresholds, the effective sensitive area of both detector types (0.05 m^2 for NaI crystal and 3×0.67 m^2 for the sum sensitive area of a single ionization counter layer in a detector point), the particle registration efficiencies from the plots of Figs. 1 and 2, and the duration of the transient burst in the vicinity of the zero point (it was set to four time intervals, i.e., to 0.64 ms for both events in Figs. 7 and 8), one can calculate the energy spectra of transient surplus radiation accountable for the bursts around the lightning trigger moment in the events of July 13 and 21. These two spectra sets are shown by the light gray (for the July 13 event) and dark gray (for July 21) colored point distributions *1* and *2* in Fig. 10; the circles correspond to the

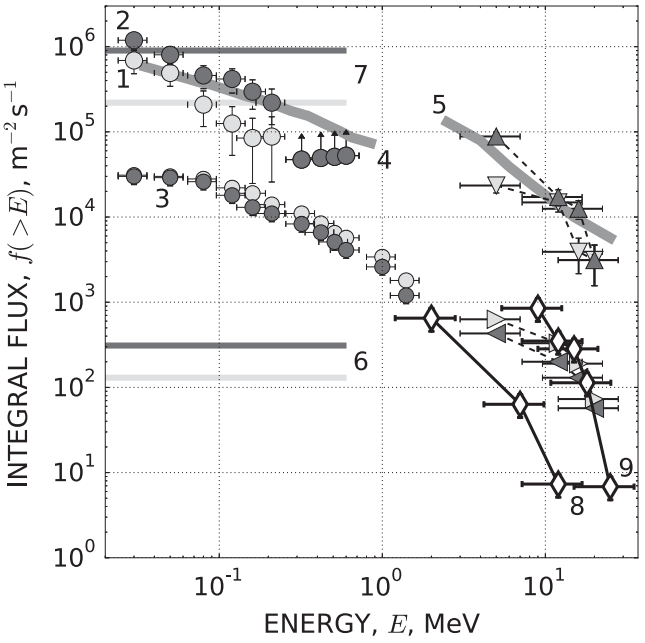

FIG. 10. Energy spectra of gamma radiation (circles) and accelerated electrons (triangles). *1* and *2*—two spectra for the transient radiation bursts around the lightning trigger moment in the high-resolution series from Figs. 7 and 8, light gray points for the July 13 event and dark gray ones for July 21; *3*—average spectra calculated over monitoring-type measurements at Tien-Shan in thunderstorm days of July 13 and 21, 2013; *4* and *5*—correspondingly, the gamma-ray and electron spectra obtained in Geant4 simulation of an electron avalanche developing in electric field of a thundercloud; *6* and *7*—the levels of neutron intensity correspondingly at a quiet time and just in the moment of transient burst on July 13 and 21; *8* and *9*—electron spectra registered in two thunderstorm events at Mount Aragats ([7], see the text).

gamma radiation, and the triangles correspond to the flux of charged particles.

Analogously, using the levels of the average counting rates in different detector types from the low-resolution time series of Fig 5, one can calculate the spectra of the radiation background which is typical for the "quiet" gaps between any transient bursts. For both stormy days of July 13 and 21, these background spectra occur being very close; they are shown correspondingly by the light and dark gray pairs of distributions, 3, in Fig. 10.

It is seen from Fig. 10 that the peak amplitude of radiation spectra in the moment of a sharp lightning-associated burst is at our observation level up to 1.5–2 orders of magnitude above its mean values, which have been routinely registered in monitoring mode without the binding to the lightning trigger.

It should be noted that the presence of short-time intensive radiation flashes just around the discharge moment may have been a cause of noticeable underestimation of their integral flux due to a limited time of

scintillation decay in inorganic NaI scintillators and insufficient operation speed of the subsequent pulse shaping electronics. Typically, the overall dead time of the pulse counting apparatus in our experiments was of the order of 1–3 μs which could result in a pileup of unresolved gamma-radiation quanta emitted in a single intensive flash. Hence, the above estimations given for the transient gamma-radiation flux must be understood in the sense of its lower possible limit.

With continuous thick gray lines 4 and 5 in Fig. 10 are shown the expected energy spectra of gamma radiation and of electron particle flows which have been generated in Geant4 simulation of the development of an electron avalanche inside a thundercloud electric field. By simulation, the concrete conditions of the Tien-Shan mountain station (the typical air pressure, density, temperature, and humidity) were taken into account; the thundercloud region with a homogeneous static 1.5 kV/m electric field was supposed to be located 2.5 km above the station's observation level, and the complete development of an electron-photon avalanche with all its products was traced since its origin due to the acceleration of a seed electron particle until attenuation in the space outside of the cloud. The simulation spectra presented in Fig. 10 correspond to the distance range of 0.3–1 km from the discharge region, like the situation in the real events of July 13 and 21, 2013. A reasonable agreement is seen in both the general power law shape and the slope between the simulated spectra and the ones restored from experimental data, which is evidence of the reliability of the procedure of particle energy determination accepted in the present experiment.

Two pairs of horizontal lines 6 and 7 in Fig. 10 indicate intensity levels of the neutron signal registered in the time gaps between electric discharge, 6, and just at the moments of transient radiation burst in the considered events of July 13 and 21, 7; see Ref. [14] for details. It is seen that a short time relative increase in neutron integral flux occurred at the moment of a burst is more than that in the electromagnetic component, and can achieve the values about 2.5–3 orders of magnitude above its background level.

Similar spectra of the transient radiation enhancements which were registered at Mount Aragats in the time of two intensive storm events on October 4, 2009, and September 19, 2010, published in Ref. [7], are shown in Fig. 10 with white diamond distributions 8 and 9. It is seen that the intensity and slope of these spectra do match satisfactorily to our background data 3 obtained in monitoring mode at the thunderstorm time. The monitoring-type organization of the measurements is generally typical for the experiments held by the Aragats group, so the mutual correspondence in spectra means an agreement between the results on thunderstorm connected particle flows registered independently at Tien-Shan and Aragats. Nevertheless, it should be noted that using an enhanced time resolution together with a strict binding of intensity measurements to the lightning trigger in the present experiment permitted investigating more precisely the fine time structure features of transient particle flow enhancements and gaining much higher estimations for their momentary integral flux.

IV. CONCLUSION

The measurements of all types of penetrating emissions were fulfilled during a thunderstorm at Tien-Shan Mountain Station. Simultaneous measurements of radio and gamma-ray emissions, high-energy electrons, neutron radiation, and the electric field and its variations are fulfilled. The measurements were done in both the monitoring mode and in the high-resolution trigger mode. This integrated approach opens up a new area of research in atmospheric physics at high energies.

We have received new information about the features of penetrating radiation in the period of thunderstorm activity, which show that the processes occurring in the thundercloud are much more complex than previously imagined. These processes are characterized by sporadic and rapid variability in both space and in time. Wherein different types of elementary particles are generated, their energy varies on many orders of magnitude. We also showed a significant difference in the magnitudes of penetrating radiation fluxes, depending on the time resolution of the recording apparatus. Measurements of characteristics of penetrating radiation in the atmospheric discharge with a high-time resolution—up to the order of tens nanoseconds—allowed us to obtain new information on the mechanism of the processes occurring in the thunderstorm atmosphere. It is especially important for a detailed study of the initial stage of the discharge. Such measurements could lead to quite unexpected results.

ACKNOWLEDGMENTS

This work was supported by the RAS Programs No. I9П and No. 10ОФ, by the RFBR Grant No. 15-45-02636, and by the projects of Kazakhstan Republick, Projects No. 0080/GF4 and No. 0003-3/PTF-15-AKMIR/0-15.

[1] M. D. McCarthy and G. K. Parks, Geophys. Res. Lett. **12**, 393 (1985).
[2] K. B. Eack, W. H. Beasley, W. David Rust, T. C. Marshall, and M. Stolzenburg, J. Geophys. Res. **101**, 29637 (1996).
[3] A. P. Chubenko, V. P. Antonova, S. Yu. Kryukov, V. V. Piskal, M. O. Ptitsyn, A. L. Shepetov, L. I. Vildanova, K. P. Zybin, and A. V. Gurevich, Phys. Lett. A **275**, 90 (2000).
[4] C. B. Moore, K. B. Eack, G. D. Aulich, and W. Rison, Geophys. Res. Lett. **28**, 2141 (2001).
[5] J. R. Dwyer and M. A. Uman, Phys. Rep. **534**, 147 (2014).
[6] J. R. Dwyer, D. M. Smith, and S. A. Cummer, Space Sci. Rev. **173**, 133 (2012).
[7] A. Chilingarian, B. Mailyan, and L. Vanyan, in *2nd International Cosmic Ray Workshop, Nor-Amberd, Armenia, 2011* (Alikhanyan National Laboratory, Yerevan, 2011), p. 151.
[8] A. V. Gurevich *et al.*, Phys. Lett. A **375**, 1619 (2011).
[9] A. P. Chubenko *et al.*, Phys. Lett. A **373**, 2953 (2009).
[10] A. V. Gurevich *et al.*, Phys. Lett. A **373**, 3550 (2009).
[11] A. V. Gurevich, A. N. Karashtin, V. A. Ryabov, A. P. Chubenko, and A. L. Shepetov, Phys. Usp. **52**, 735 (2009).
[12] Geant4 Collaboration, Nucl. Instrum. Methods Phys. Res., Sect. A **506**, 250 (2003).
[13] A. V. Gurevich *et al.*, Phys. Rev. Lett. **108**, 125001 (2012).
[14] A. V. Gurevich *et al.*, Atmos. Res. **164–165**, 339 (2015).
[15] A. V. Gurevich *et al.*, Phys. Lett. A **325**, 389 (2004).
[16] J. Clay, H. F. Jongen, and A. J. J. Aarts, Physica (Amsterdam) **18**, 801 (1952).
[17] M. L. Gaso, N. Servantes, and V. H. Espindola, Radiation Measurements **23**, 225 (1994).
[18] U. B. Jayanthi *et al.*, in *Proceedings of the 29th International Cosmic Ray Conference, Pune, 2005* (Tata Institute of Fundamental Research, Mumbai, 2005), p. 101.
[19] N. M. Salikhov, G. D. Pak, O. N. Kryakunova, A. P. Chubenko, and A. L. Shepetov, in *Proceeding of the 32nd International Cosmic Ray Conference, Beijing, China, 2011* (Local Organizing Committee of ICRC 2011, Beijing, 2011), Vol. 11, p. 368.